Article

Comparative Radiation Response of GaN and Ga_2O_3 Exposed to Ground-Level Neutrons

Jean-Luc Autran [1,2,*] and Daniela Munteanu [1]

[1] Aix-Marseille Univ, CNRS, IM2NP (UMR 7334), 13397 Marseille CEDEX 20, France; daniela.munteanu@univ-amu.fr
[2] Univ. Rennes, CNRS, IPR (UMR 6251), 35042 Rennes CEDEX, France
* Correspondence: jean-luc.autran@univ-rennes.fr

Abstract: In this work, the radiation response of bulk GaN and Ga_2O_3 materials exposed to ground-level neutrons is studied by Geant4 numerical simulation, considering the whole atmospheric neutron spectrum at sea level, from thermal to high energies (GeV). The response of the two materials is compared in terms of the number and type of interactions and the nature of the secondary products produced, particularly in nuclear reactions. Our results highlight the importance of $^{14}N(n,p)^{14}C$ neutron capture in the radiation response of GaN, leading to large differences in the behavior of the two materials in terms of susceptibility to thermal and intermediate-energy (below 1 MeV) neutrons.

Keywords: atmospheric neutrons; neutron–semiconductor interactions; wide-bandgap semiconductors; gallium nitride; gallium oxide; nuclear reactions; Geant4; numerical simulations; radiation effects on electronics; single-event effects

Citation: Autran, J.-L.; Munteanu, D. Comparative Radiation Response of GaN and Ga_2O_3 Exposed to Ground-Level Neutrons. *Crystals* **2024**, *14*, 128. https://doi.org/10.3390/cryst14020128

Academic Editors: Ludmila Isaenko and Evgeniy N. Mokhov

Received: 27 December 2023
Revised: 21 January 2024
Accepted: 24 January 2024
Published: 26 January 2024

Copyright: © 2024 by the authors. Licensee MDPI, Basel, Switzerland. This article is an open access article distributed under the terms and conditions of the Creative Commons Attribution (CC BY) license (https://creativecommons.org/licenses/by/4.0/).

1. Introduction

In the ever-evolving semiconductor landscape, gallium nitride (GaN) and gallium oxide (Ga_2O_3) have emerged as key wide-bandgap semiconductors in applications ranging from power electronics to optoelectronics, and their unique properties promise new levels of performance and efficiency [1–3]. Gallium is the common element in GaN and Ga_2O_3, but each material has its own characteristics. On the one hand, GaN, a compound of gallium and nitrogen, has attracted considerable interest in the world of electronics due to its exceptional electron mobility, thermal stability, and high breakdown voltage [4,5]. This combination of properties makes GaN a preferred choice for applications that require high frequency and high-power operation, such as radio frequency (RF) amplifiers, power supplies and LED lighting. GaN is also very interesting for its stability and robustness in radiation environments and is used for nuclear particle detection [6–10]. On the other hand, Ga_2O_3 is another semiconductor with a wide bandgap that has received increasing attention in recent years. Its unique crystalline structure, large bandgap, and excellent electrical insulating properties make it suitable for a variety of applications, including power electronics, UV photodetectors, and sensors [11–13]. Ga_2O_3's potential to handle high voltages and temperatures while maintaining efficiency makes it a strong candidate for the next generation of power devices.

In recent years, the interest in these wide-bandgap materials for space and avionics applications, or for applications in extreme conditions, has led to the emergence of dedicated studies of the radiation response of technologies based on these materials, especially with respect to the response to thermal or fast neutrons [14–20]. In this context, the aim of this work is to investigate the radiation response of both GaN and Ga_2O_3 exposed to the natural radiation background at sea level consisting of atmospheric neutrons with energies ranging from thermal to GeV. The response of electronic devices made from these materials to radiation has been the focus of most of the research in this area [21–25]. The effects of neutron irradiation on bulk GaN or Ga_2O_3 at the material level (i.e., not integrated

into electronic devices) have been studied only to a limited extent. We can cite previous studies [15,17,26,27] that have investigated the susceptibility of several materials from the group IV or III-V compound materials, including GaN. However, these studies have limitations with respect to (i) the energy of the incoming neutrons, because the study in [27] simulates only neutrons issued from deuterium–deuterium or deuterium–tritium fusion reactions (i.e., monoenergetic neutrons with energies of 2.45 MeV and 14 MeV), and the other studies [15,17,26] include only the high-energy neutron part of the neutron spectrum at ground level; (ii) the energy of the secondary particles resulting from the interactions of atmospheric neutrons with the material (due to a limiting energy threshold, which is considered in [26]); and (iii) the event statistics in [26], because a relatively small number of incoming neutrons affect the simulation results. As far as Ga_2O_3 is concerned, to the best of our knowledge, there is no study in the literature on the effect of atmospheric neutrons at the material level. In this work, we investigate and compare the effects of sea-level atmospheric neutrons on GaN and Ga_2O_3 bulk materials. The comparison of the atmospheric neutron susceptibility of GaN and Ga_2O_3 is quantified in terms of the number and type of interactions (elastic, inelastic, nuclear), and also in terms of the nature and number of secondaries (protons, alpha, . . .) produced in nuclear reactions. In contrast to previous studies, in this work, we consider the entire neutron spectrum at sea level, covering the energy range from the thermal to the GeV range. Moreover, the analysis was conducted without any restrictions (i.e., filtering) on the energy of secondary products and a significant number of incident neutrons was simulated. The interaction events between atmospheric neutrons and semiconductor target materials, representing 25×10^6 h of irradiation in the natural background at sea level, are simulated using the Monte Carlo radiation transport code Geant4 [28–30]. A dedicated source of atmospheric neutrons and large databases containing complete information on tens of thousands of interaction events have been created using this code.

The paper is organized as follows: Section 2 begins with a presentation of the bulk properties of GaN and Ga_2O_3 materials and the sea-level neutron spectrum used as the neutron source in the simulation. Next, the direct calculation of the number of neutron–material interactions is described in detail, as well as the more comprehensive and complex Monte Carlo numerical simulation (using Geant4) of the neutron–target interactions. In Section 3, we present the detailed results of these simulations in terms of the number and type of interactions. In this section, an extensive analysis involves the energy distribution of secondary products as a function of the energy range of the incident neutron spectrum. Finally, Section 4 presents a detailed discussion of the response of the two materials to atmospheric neutrons in terms of the number of interactions likely to induce significant single event effects (SEEs) in a device or circuit.

2. Materials and Methods

2.1. Materials Properties

For this study, we considered bulk materials with natural isotopic compositions. Gallium (Z = 31) has two stable isotopes, ^{69}Ga and ^{71}Ga, with natural abundances of 60.1% and 39.9%, respectively. Nitrogen (Z = 7) and oxygen (Z = 8) have two and three stable isotopes, respectively, but we consider only ^{14}N and ^{16}O because they represent the vast majority (>99.6%) of naturally occurring nitrogen and oxygen, respectively.

Table 1 summarizes the other main physical and atomic properties of bulk GaN and Ga_2O_3 considered in this work [31,32].

Table 1. Main properties of bulk GaN and Ga_2O_3.

Properties (300 K)	β-Ga_2O_3	GaN
Bandgap (eV)	4.6–4.9	3.39
Density (g/cm^3)	5.96	6.15
Atoms (cm^{-3})	9.45×10^{22}	8.85×10^{22}
$\varepsilon_{e,h}$ (eV) [1]	15.6	8.9

[1] Energy required to create an electron–hole pair.

2.2. Atmospheric Neutron Source

The atmospheric neutron flux is needed to calculate the neutron interactions with the materials under study. In this work, we use as a reference input spectrum the differential neutron flux induced by cosmic rays measured by Goldhagen at Yorktown Heights [33,34], shown in Figure 1. The spectrum is divided into three parts: part I (<1 eV) corresponds to thermal and low-energy neutrons, part II (between 1 eV and 1 MeV) to intermediate-energy neutrons, and part III (>1 MeV) to high-energy neutrons. The total neutron flux corresponding to each part is given in the figure. The integral flux over the whole spectrum is 43.6 neutrons per cm^2 and per hour (mid-level solar activity, outdoors) [35].

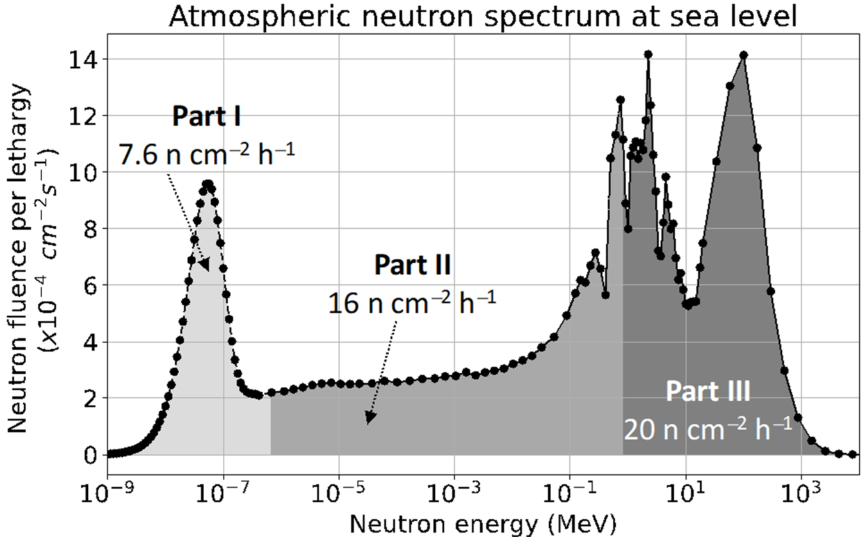

Figure 1. Complete reference atmospheric neutron spectrum measured on the roof of the IBM Watson Research Center main building (lethargic representation) [33]. Numerical data courtesy from Paul Goldhagen (U.S. Department of Homeland Security).

2.3. Direct Calculation of the Number of Interactions

In a first approach, the susceptibility of GaN and Ga_2O_3 materials to atmospheric neutrons was evaluated from the direct calculation of the number of neutron–material interactions in a target representative of a microelectronic circuit, following a method described in [15]. We considered a parallelepiped target (surface S = 1 cm^2, thickness t = 20 µm) of bulk GaN or Ga_2O_3 exposed to incident neutrons arriving perpendicular to its largest surface. The number of nuclear interactions R_n (s^{-1}·cm^{-2}) in the target is given by

$$R_n = N \times t \times \int_{E_{min}}^{E_{max}} \sigma_n(E) \frac{d\phi}{dE} dE \quad (1)$$

where σ_n(E) (cm^2) is the GaN or Ga_2O_3 neutron cross-section, N is the number of atoms (cm^{-3}) given in Table 1, t is the target thickness (in cm), $d\phi/dE$ is the differential atmospheric neutron flux (cm^{-2}·s^{-1}·MeV^{-1}) at ground level (see Figure 1), and E_{min} and E_{max} are the limits of the energy domain considered (see Figure 1).

In Equation (1), GaN or Ga_2O_3 neutron cross-sections were evaluated from the combination of those of ^{69}Ga, ^{71}Ga, ^{14}N, and ^{16}O given by the evaluated nuclear data library ENDF/B-VIII.020 [36,37] (supplemented with data from JENDL-4.021 [38] for Ga isotopes in the range 20–200 MeV) and considering the material stoichiometry. The individual nuclear cross-sections as a function of neutron energy are shown in Figure 2 for the gallium isotopes and in Figure 3 for the ^{14}N and ^{16}O isotopes.

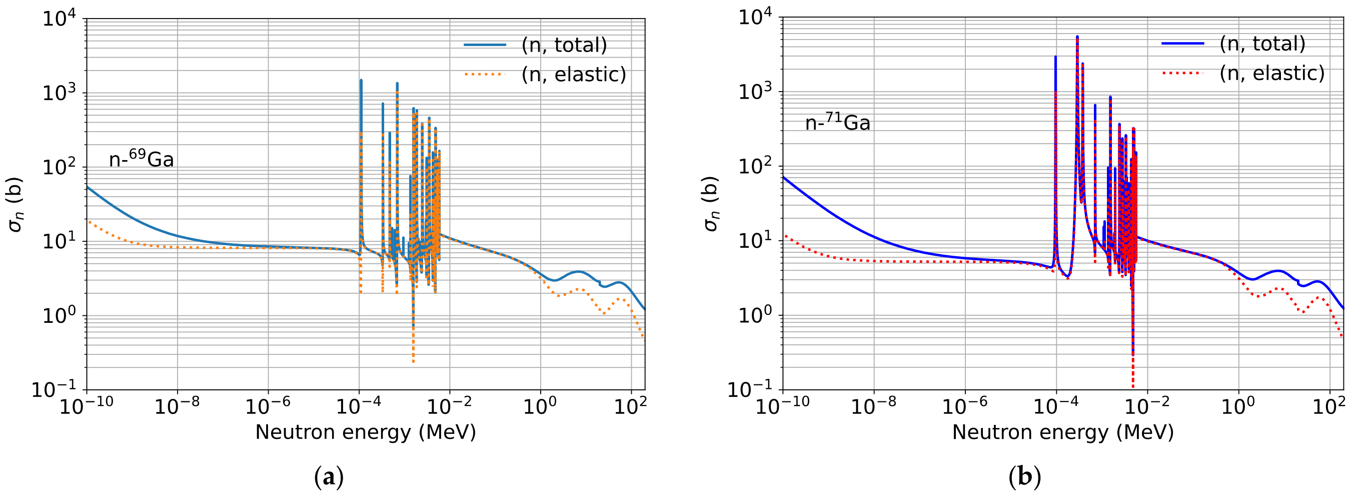

Figure 2. Neutron cross-sections for ^{69}Ga and ^{71}Ga isotopes. Numerical data from ENDF/B-VIII.020 and JENDL-4.021 evaluated nuclear data libraries. (**a**) ^{69}Ga; (**b**) ^{71}Ga.

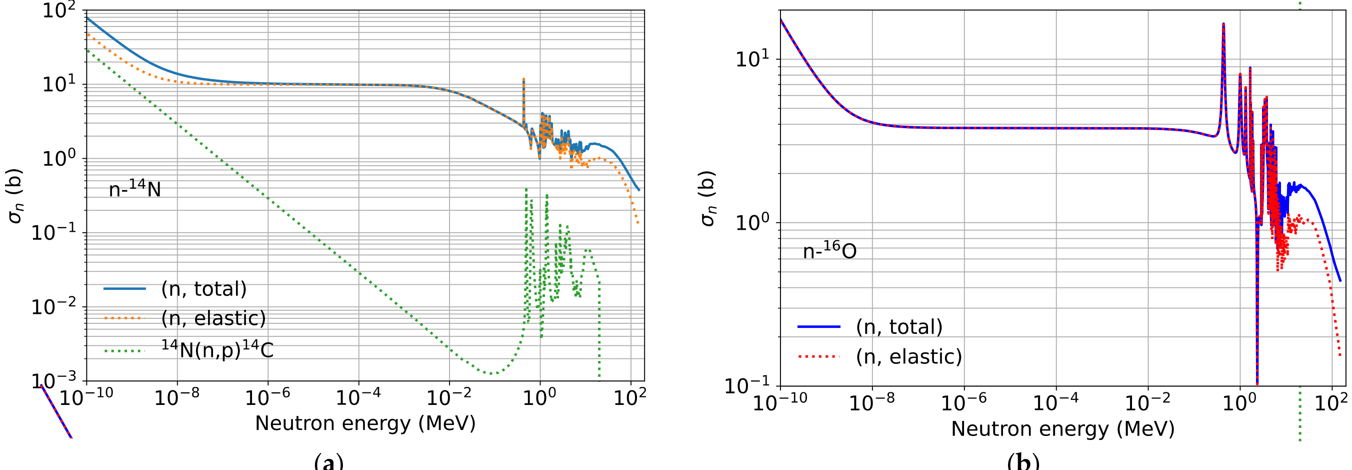

Figure 3. Neutron cross-sections for ^{14}N and ^{16}O isotopes. Numerical data from ENDF/B-VIII.020 and JENDL-4.021 evaluated nuclear data libraries. (**a**) ^{14}N; (**b**) ^{16}O.

2.4. Geant4 Simulation Details

To complement this direct calculation and to further analyze the reaction secondary products, we performed extensive numerical simulations using the Monte Carlo Radiation Transport Code Geant4 [28–30] version 10.7.2, considering the precompiled physics list QGSP_BIC_HP. This physics list includes a binary cascade, pre-compound, and various de-excitation models for hadrons, standard electromagnetic models, and high-precision neutron models used for neutrons up to 20 MeV. The simulations considered the same geometry target as previously defined, and the same neutron flux spectrum (per energy domains I, II and III), which was imported into Geant4 through the General Particle Source (GPS) module [39] to randomly generate incident neutrons mimicking this natural neutron background. For each part of the spectrum, the simulations considered a number of incoming neutrons equivalent to 25×10^6 h of natural radiation exposure. This corresponds to 1.9×10^8 primary neutrons generated by the Geant4 GPS source for part I, 4×10^8 neutrons for part II, and 5×10^8 neutrons for part III. Each Geant4 simulation run (1 per material and per part of the spectrum, i.e., 6 databases in total) produces a unique output file containing all the information related to each interaction of neutrons with the target material. This information includes the nature of the interaction, the spatial coordinates of the reaction vertex, and a complete list of the secondary particles produced during the interaction (along with the energy and emission direction vector for each of these emitted

particles). Gamma photons, neutral and light particles (e−, e+, η, neutral pions), which are not able to induce significant effects in the semiconductor material in the sense of single events in microelectronics, are eliminated in a post-treatment process [40].

3. Results

3.1. Number of Interactions

Figure 4 shows the results of these direct calculations (denoted ENDF/JENDL) for both the GaN and Ga_2O_3 targets (1 cm^2 × 20 µm) exposed to parts I, II, and III of the atmospheric spectrum defined in Figure 1.

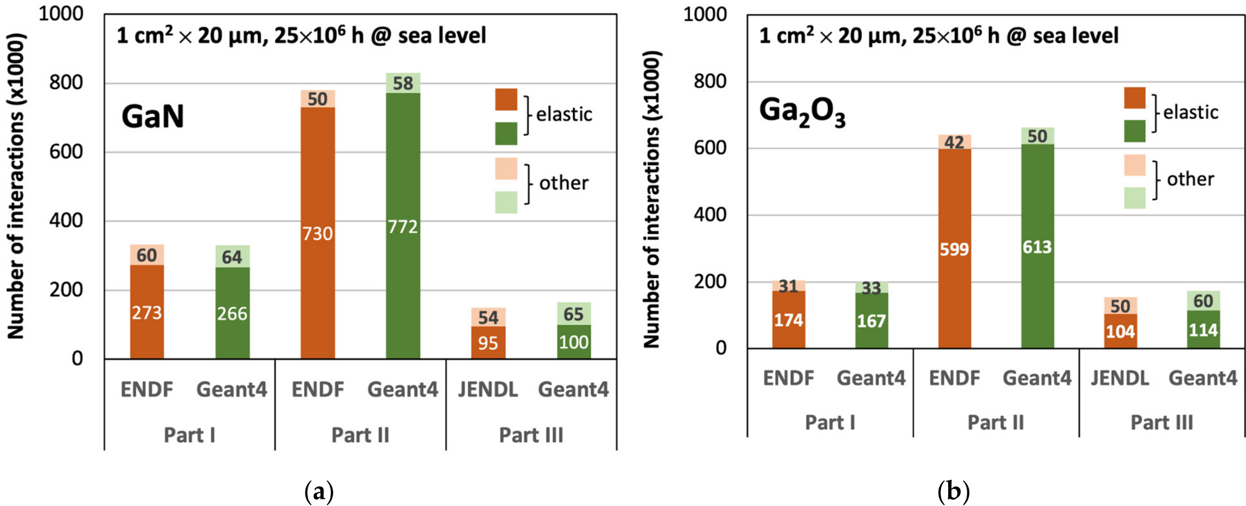

Figure 4. Number of neutron interactions (thousands) in GaN and Ga_2O_3 bulk targets (1 cm^2 × 20 µm) exposed to part I, II, or III of the neutron atmospheric spectrum of Figure 1 during 25 × 10^6 h. ENDF/JENDL denotes direct calculation from Equation (1) using evaluated nuclear libraries, Geant4 denotes numerical simulation using the Monte Carlo radiation transport code Geant4. Interactions have been partitioned into two classes: elastic and other, which includes inelastic, capture and other neutron-induced nuclear reactions. (**a**) GaN; (**b**) Ga_2O_3.

These values are expressed for an exposure equivalent to 25 × 10^6 h under natural conditions at ground level. Overall, GaN shows much more neutron interactions below 1 MeV than Ga_2O_3: +62.5% for part I and +21.7% for part II, respectively. Above 1 MeV, the two materials show approximately the same number of interactions. Elastic interactions represent the largest contributions for the three energy ranges and for both materials: 82% for GaN and 85% for Ga_2O_3 exposed to part I of the spectrum, 93.5% for both targets in part II, and 63.6% for GaN and 67.5% for Ga_2O_3 in part III. This greater susceptibility of GaN to neutrons below 1 MeV compared to Ga_2O_3 is due to differences in the sizes of the neutron-^{14}N and neutron-^{16}O cross-sections in the energy range between 10^{-4} and 1 eV, as shown in Figure 3. Schematically, there are two times more neutron interactions with ^{14}N than with ^{16}O for part I and 1.5 times more for part II. In fact, for part II, which is dominated by the elastic interaction, the elastic neutron-^{14}N cross-section is 1.7 times larger than that of ^{16}O, and for part I, in addition to elastic events, ^{14}N can also capture thermal neutrons and release low-energy protons through the ^{14}N(n,p)^{14}C reaction. This explains the increased number of neutron interactions with ^{14}N, twice that with ^{16}O for this energy range (part I).

Figure 4 also shows the comparison of the number of interactions derived from the Geant4 simulations with the number of interactions previously obtained from direct calculations using Equation (1). There is good agreement between the two sets of data, with a maximum difference of 2% for Part I, 6% for Part II, and 13% for Part III. This is because the upper limit of the integral (term E_{max} in Equation (1)) was limited to 200 MeV, corresponding to the energy range of the cross-section values available in the JENDL/4.0

library, while Geant4 generates and transports neutrons with energies up to the maximum of the spectrum, i.e., up to 10 GeV.

3.2. Type of Interactions

To take the analysis one step further, Figure 5 provides details of the interactions labeled "other" in Figure 4, i.e., interactions that are not elastic.

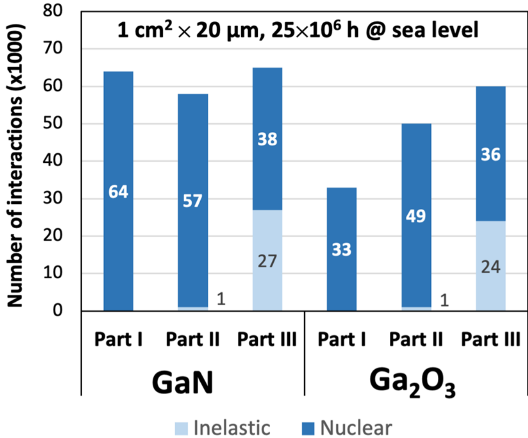

Figure 5. Number of inelastic and nuclear neutron interactions (thousands) in GaN and Ga_2O_3 bulk targets (1 cm^2 × 20 µm) exposed to part I, II, or III of the neutron atmospheric spectrum of Figure 1 during 25 × 10^6 h.

We distinguish in this category the inelastic interactions (n,n') and all the other neutron–nucleus interactions, such as X(n,γ)Y, (n,α), (n,p), (n,fission), etc., which are collectively referred to as "nuclear reactions" (or nonelastic reactions). We note that there are twice as many nuclear reactions for GaN compared to Ga_2O_3 for thermal and low-energy neutrons (Part I), +16% for intermediate-energy neutrons (Part II), and about the same number and proportion of inelastic and nuclear reactions for high-energy neutrons (Part III).

Table 2 gives the details of some of these reactions and their occurrence as a function of the energy range considered. The occurrences of elastic interactions are also included in Table 2 for comparison. Unlike elastic reactions, which are characterized by a Q-value of zero (i.e., there is no release or absorption of energy), the ^{69}Ga(n,γ)^{70}Ga, ^{71}Ga(n,γ)^{72}Ga, ^{14}N(n,γ)^{15}N, and ^{14}N(n,p)^{14}C reactions are exothermic and are characterized by large positive Q-values of 9.8 MeV, 9.5 MeV, 13.6 MeV, and 626 keV, respectively.

Table 2. Occurrence of elastic and some special capture reactions in GaN and Ga_2O_3 and their frequency (thousands).

Reaction	Part I		Part II		Part III	
	GaN	Ga_2O_3	GaN	Ga_2O_3	GaN	Ga_2O_3
^{69}Ga elastic	68	58	182	158	38	33
^{71}Ga elastic	27	23	320	278	25	22
^{14}N elastic	171	-	270	-	37	-
^{16}O elastic	-	86	-	177	-	59
^{69}Ga(n,γ)^{70}Ga	14	12	25	22	1	1
^{71}Ga(n,γ)^{72}Ga	25	21	31	27	0	0
^{14}N(n,γ)^{15}N	1	-	0	-	0	-
^{14}N(n,p)^{14}C	24	-	1	-	1	-

3.3. Secondary Products

Secondary products released in these reactions have kinetic energies (much) greater than the energy of the incoming neutrons. This is clearly visible in the energy histograms

computed from the Geant4 databases for both materials and for the three parts of the spectrum. Figure 6 shows the energy histograms for part I of the neutron spectrum and for Ga_2O_3 (Figure 6a) and GaN (Figure 6b).

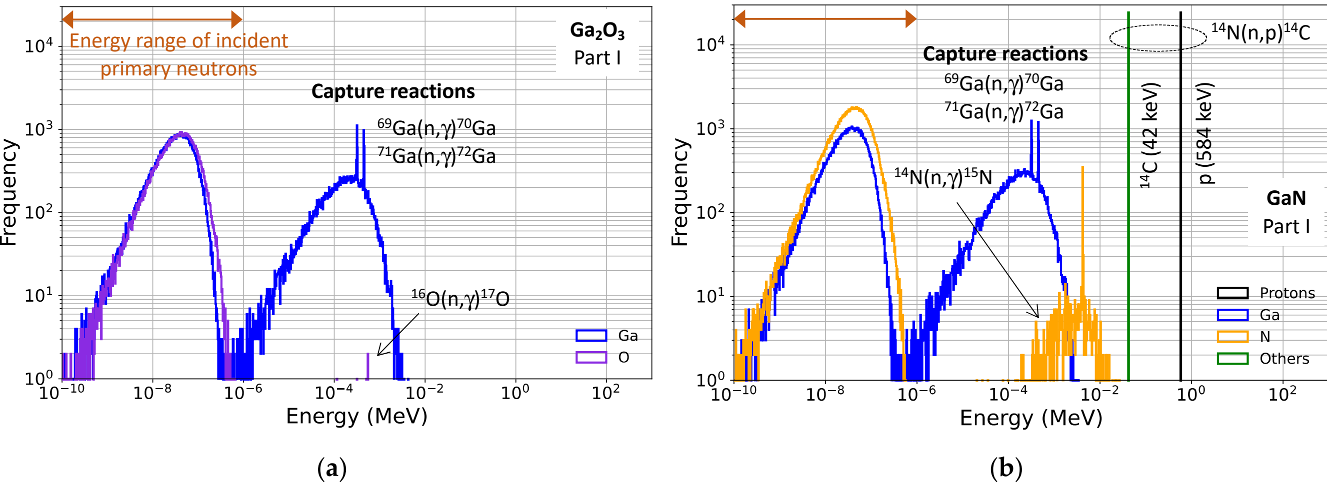

(**a**) (**b**)

Figure 6. Histograms in energy of the secondary products produced in the GaN and Ga_2O_3 bulk targets (1 cm^2 × 20 µm) exposed to part I of the neutron atmospheric spectrum of Figure 1 during 25 × 10^6 h. (**a**) Ga_2O_3; (**b**) GaN.

Two distinct distributions of secondary products are visible for Ga_2O_3 and GaN for part I: the distribution of elastic recoil nuclei (Ga and O for Ga_2O_3, Ga and N for GaN), which has a maximum just below 10^{-7} eV, and a second distribution of Ga nuclei produced in $^{69}Ga(n,\gamma)^{70}Ga$ and $^{71}Ga(n,\gamma)^{72}Ga$ reactions from the eV to the keV ranges. For GaN specifically (Figure 6b), the additional contributions from $^{14}N(n,\gamma)^{15}N$ and $^{14}N(n,p)^{14}C$ reactions give a distribution of ^{15}N in the keV range and two monoenergetic distributions of ^{14}C at 42 keV and protons at 584 keV, respectively. Note that there is no significant contribution from the equivalent reaction for ^{16}O; the reaction $^{16}O(n,\gamma)^{17}O$ occurs only a few times (see Figure 6a). The release of these products via the capture of neutrons by nitrogen is potentially problematic for the radiation reliability of any material or device containing nitrogen, as recently shown by Coronetti et al. [41] in the context of silicon technologies with nitride layers. In the present study, this issue primarily concerns GaN devices. The released products can transfer their energy to the semiconductor and generate significant electrical charges in GaN: 584 keV protons will transfer more than 10 fC of charge each in GaN, and 42 keV ^{14}C will transfer nearly 0.8 fC.

Figure 7 shows the energy histograms for part II of the neutron spectrum, for Ga_2O_3 (Figure 7a) and GaN (Figure 7b). In part II of the spectrum, the $^{14}N(n,p)^{14}C$ reaction channel still produces ^{14}C nuclei and protons (Figure 7b), but in smaller amounts, which also makes GaN more sensitive to radiation than Ga_2O_3 in terms of secondary products that are likely to produce single events.

Finally, the energy histograms for part III of the spectrum (Figure 8a,b), as well as Figure 5, show that for high-energy neutrons above 1 MeV, GaN and Ga_2O_3 are relatively equivalent in terms of the number and type of interactions, as well as the energy distributions of the secondaries (recoils, protons, alpha particles, and other heavy fragments).

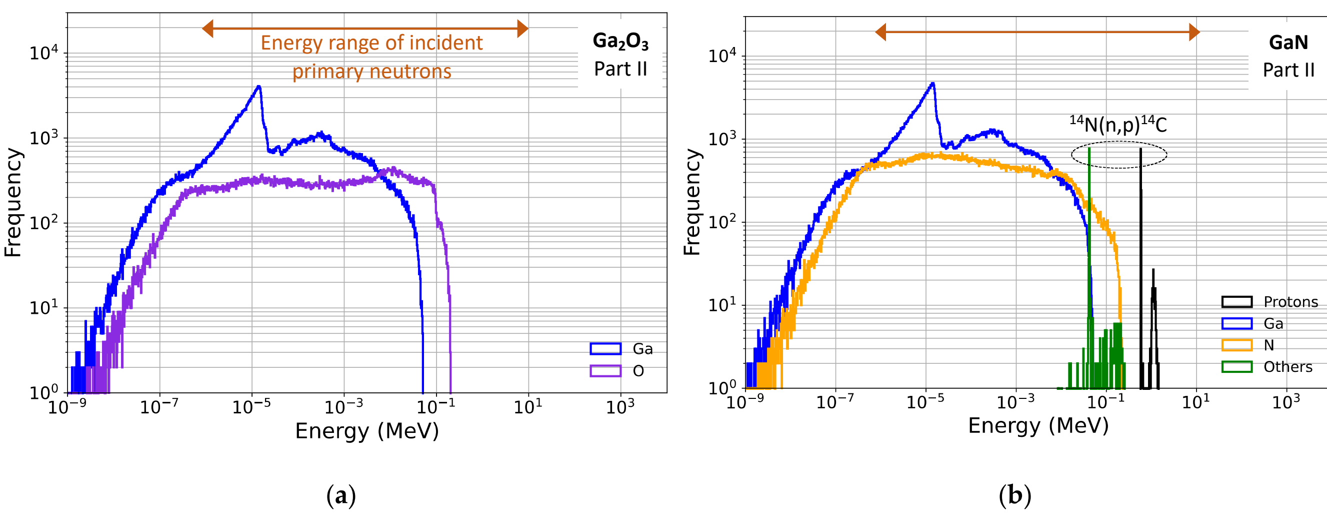

Figure 7. Histograms in energy of the secondary products produced in the GaN and Ga_2O_3 bulk targets (1 cm^2 × 20 µm) exposed to part II of the neutron atmospheric spectrum of Figure 1 during 25 × 10^6 h. (**a**) Ga_2O_3; (**b**) GaN.

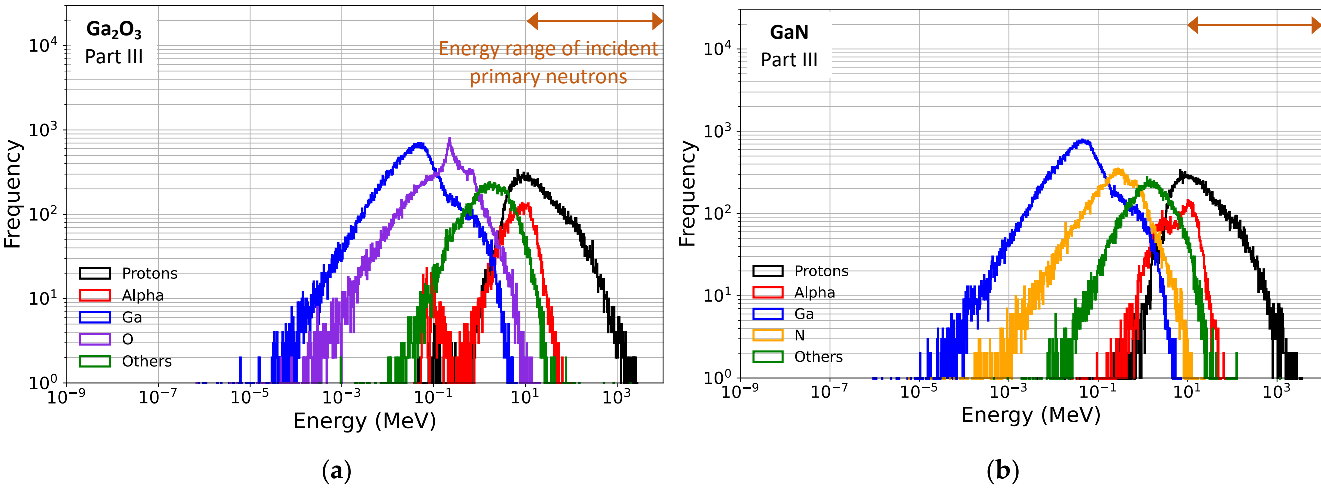

Figure 8. Histograms in energy of the secondary products produced in the GaN and Ga_2O_3 bulk targets (1 cm^2 × 20 µm) exposed to part III of the neutron atmospheric spectrum of Figure 1 during 25 × 10^6 h. (**a**) Ga_2O_3; (**b**) GaN.

Quantitative details on the production of secondary products, classified as a function of their atomic number, are given in Figure 9 for both target materials. These distributions show that GaN and Ga_2O_3 are quasi-equivalent in terms of proton (Z = 1) and alpha particle (Z = 2) emission, with a slightly higher production (+10%) of alphas in GaN due to more (n, α) reaction channels with ^{14}N than with ^{16}O. For Z > 13, GaN has a higher production rate of secondary products than Ga_2O_3, mainly because these fragments are emitted from neutron–Ga interactions and the Ga atomic concentration is 17% higher in GaN than in Ga_2O_3.

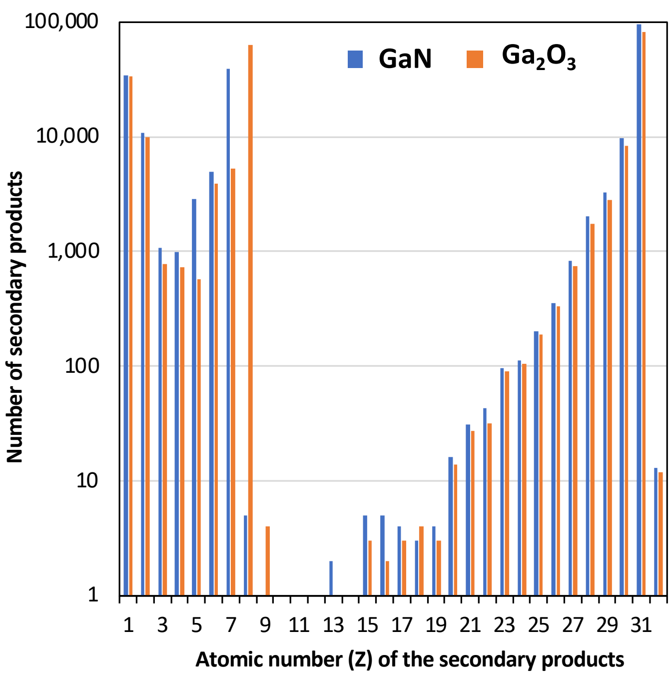

Figure 9. Atomic number (Z) distribution of all secondary products produced in both GaN and Ga_2O_3 target (1 cm^2 × 20 µm) exposed to the full neutron atmospheric spectrum of Figure 1 for 25 × 10^6 h.

4. Discussion

The results presented above allow us to discuss the response of Ga_2O_3 and GaN to atmospheric neutrons in terms of the number of interactions that are likely to cause significant SEEs in a device or circuit. We begin by recalling the mechanisms of single-event production after neutron–material interactions that release secondary products (charged light particles and recoil nuclei). Through direct ionization, a mechanism in which charged particles interact primarily with the electrons of the material's atoms, these secondary products transfer energy to the material [35]. The ionization mechanism produces many excited energetic electrons (delta rays), which usually have enough energy to ionize other atoms. These electrons produce a cascade of secondary electrons that lose energy, creating a column of electron–hole pairs along the path of the particle [40]. Thus, the transferred energy is essentially converted into electron–hole pairs. The amount of energy required to create an electron–hole pair depends on the bandgap of the material (15.6 eV for Ga_2O_3 and 8.9 eV for GaN, see Table 1). Once the dense column of electron–hole pairs is formed, three different mechanisms are involved in the evolution and the transport of these charges: drift in the device regions exposed to an electric field, ambipolar diffusion in the neutral zones, and recombination with other mobile carriers [35]. The transported charges are then collected by elementary structures in the device (such as reverse-biased junctions). This collection mechanism results in a parasitic transient current that is injected into the circuit node affected by the particle, causing circuit disturbances such as SEEs [35].

Returning to the energy distributions of the secondary products issued from neutron interactions with Ga_2O_3 and GaN (Figures 6–8), a significant fraction of these products have very low energies, especially in parts I and II of the incident neutron spectrum. Such low-energy particles are likely to create (by energy transfer in the semiconductor) very few electron–hole pairs in materials, and will therefore have no effect on the operation of components and circuits. Consequently, it seems appropriate to "filter" the energy of the reactions in order to eliminate all those that cannot induce a minimum number of electron–hole pairs in the target materials. Figure 10 shows the remaining number of events when all the reactions that are not able to produce at least 1000 electron-hole pairs have been eliminated. This threshold value is more or less arbitrary and corresponds to

a charge of 0.16 fC, which is in the order of magnitude of critical charges in current static random-access memories (SRAMs) [35]. We remind the reader that the critical charge for memory circuits is defined as the minimum amount of collected charge that causes a device node to change its logical state, leading to a single event upset [42].

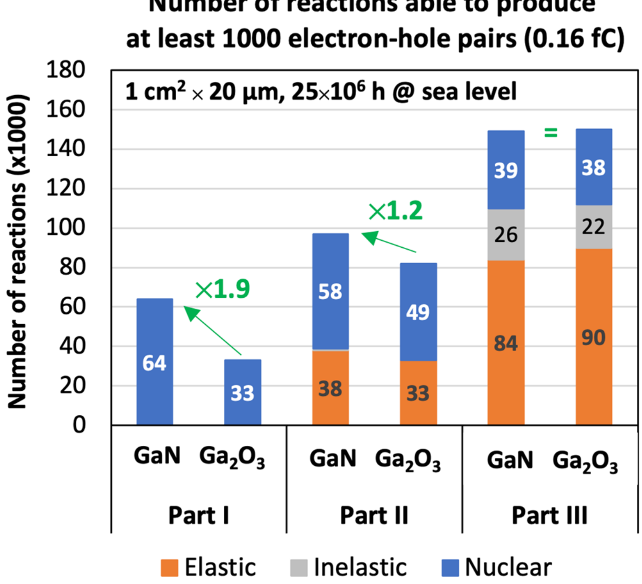

Figure 10. Number of neutron reactions able to produce at least 1000 electron–hole pairs in both GaN and Ga_2O_3 target (1 cm^2 × 20 µm) exposed to the full neutron atmospheric spectrum of Figure 1 during 25 × 10^6 h.

This filtering has the effect of eliminating virtually all of the recoil nuclei in part I of the spectrum and a very large fraction of those in part II. Consequently, for part I, only the nuclei produced in the nuclear (capture) reactions remain. For part II, the nuclei not removed are those produced in capture reactions, with an additional contribution from the most energetic recoil nuclei. For Part III, only the less energetic recoil nuclei are eliminated.

Finally, Figure 10 shows a direct comparison of the atmospheric neutron response of the two materials in terms of the number of interactions likely to cause significant single event effects in a device or circuit. The results show that GaN is almost twice as sensitive as Ga_2O_3 to the first part of the spectrum and 20% more sensitive to the second part of the spectrum. At higher energies (>1 MeV), the two materials are fully equivalent. The consequences of these results, derived at the material level, are potentially important in terms of technological choices; for applications where thermal or low-energy neutrons are a major constraint, Ga_2O_3-based electronics should be preferred; while at high energies (above 1 MeV), GaN-based or Ga_2O_3-based electronics are equivalent in terms of neutron susceptibility. Another practical consequence is that GaN-based electronics should be used only with special precautions (systematic use of absorbing materials, type B4C) to eliminate thermal neutrons, a less essential precaution for Ga_2O_3-based electronics (which is more tolerant to thermal neutrons).

5. Conclusions

In conclusion, this study provided a careful comparison of the radiation response of bulk GaN and Ga_2O_3 materials exposed to ground-level neutrons from thermal to high energies (GeV). The response of these two materials was evaluated by direct calculation from nuclear libraries and from extensive Geant4 numerical simulation. Our results highlight the relative equivalence of both materials exposed to the higher part of the atmospheric neutron spectrum above 1 MeV and the enhanced susceptibility of GaN to thermal neutrons compared to Ga_2O_3, mainly due to the presence of nitrogen and its interaction with neutrons via the exothermic $^{14}N(n,p)^{14}C$ capture reaction. This study should shed light

on the choice of GaN or Ga_2O_3 as the semiconductor material of the targeted electronic solution, depending on the intended application and the radiation context, whether natural or artificial.

Author Contributions: Conceptualization, J.-L.A. and D.M.; methodology, J.-L.A. and D.M.; software, J.-L.A. and D.M.; formal analysis, J.-L.A. and D.M.; investigation, J.-L.A. and D.M.; writing—review and editing, J.-L.A. and D.M.; visualization, J.-L.A. and D.M. All authors have read and agreed to the published version of the manuscript.

Funding: This research received no external funding.

Data Availability Statement: The data presented in this study are available on reasonable request from the corresponding authors.

Conflicts of Interest: The authors declare no conflicts of interest.

References

1. Tsao, J.Y.; Chowdhury, S.; Hollis, M.A.; Jena, D.; Johnson, N.M.; Jones, K.A.; Kaplar, R.J.; Rajan, S.; Van de Walle, C.G.; Bellotti, E.; et al. Ultrawide-Bandgap Semiconductors: Research Opportunities and Challenges. *Adv. Electron. Mater.* **2018**, *4*, 1600501. [CrossRef]
2. Dahiya, S.; Kaur, D.; Ghosh, A.; Kumar, M. A strategic review on gallium oxide based power electronics: Recent progress and future prospects. *Mater. Today Commun.* **2022**, *33*, 104244.
3. Xu, M.; Wang, D.; Fu, K.; Mudiyanselage, D.H.; Fu, H.; Zhao, Y. A review of ultrawide bandgap materials: Properties, synthesis and devices. *Oxf. Open Mater. Sci.* **2022**, *2*, itac004. [CrossRef]
4. Ding, X.; Zhou, Y.; Cheng, J. A review of gallium nitride power device and its applications in motor drive. *CES Trans. Electr. Mach. Syst.* **2019**, *3*, 54–64. [CrossRef]
5. Udabe, A.; Baraia-Etxaburu, I.; Diez, D.G. Gallium Nitride Power Devices: A State of the Art Review. *IEEE Access* **2023**, *11*, 48628–48650. [CrossRef]
6. Kumar, S.; Reshi, B.A.; Varma, R. Comparison of Silicon, Germanium, Gallium Nitride, and Diamond for using as a detector material in experimental high energy physics. *Results Phys.* **2018**, *11*, 461–474. [CrossRef]
7. Wang, J.; Mulligan, P.; Brillson, L.; Cao, L.R. Review of using gallium nitride for ionizing radiation detection. *Appl. Phys. Rev.* **2015**, *2*, 031102. [CrossRef]
8. Pearton, S.J.; Ren, F.; Patrick, E.; Law, M.E.; Polyakov, A.Y. Review—Ionizing Radiation Damage Effects on GaN Devices. *ECS J. Solid State Sci. Technol.* **2016**, *5*, Q35–Q60. [CrossRef]
9. Zhang, Y.; Dadgar, A.; Palacios, T. Gallium nitride vertical power devices on foreign substrates: A review and outlook. *J. Phys. D Appl. Phys.* **2018**, *51*, 273001. [CrossRef]
10. Zhou, C.; Melton, A.G.; Burgett, E.; Hertel, N.; Ferguson, I.T. Neutron detection performance of gallium nitride based semiconductors. *Sci. Rep.* **2019**, *9*, 17551. [CrossRef]
11. Qiao, R.; Zhang, H.; Zhao, S.; Yuan, L.; Jia, R.; Peng, B.; Zhang, Y. A state-of-art review on gallium oxide field-effect transistors. *J. Phys. D Appl. Phys.* **2022**, *55*, 383003. [CrossRef]
12. Zhang, M.; Liu, Z.; Yang, L.; Yao, J.; Chen, J.; Zhang, J.; Wei, W.; Guo, Y.; Tang, W. β-Ga_2O_3-Based Power Devices: A Concise Review. *Crystals* **2022**, *12*, 406. [CrossRef]
13. Xue, H.; He, Q.; Jian, G.; Long, S.; Pang, T.; Liu, M. An Overview of the Ultrawide Bandgap Ga_2O_3 Semiconductor-Based Schottky Barrier Diode for Power Electronics Application. *Nanoscale Res. Lett.* **2018**, *13*, 290. [CrossRef] [PubMed]
14. Pearton, S.; Aitkaliyeva, A.; Xian, M.; Ren, F.; Khachatrian, A.; Ildefonsorosa, A.; Islam, Z.; Rasel, M.; Haque, A.; Polyakov, A.; et al. Review—Radiation Damage in Wide and Ultra-Wide Bandgap Semiconductors. *ECS J. Solid State Sci. Technol.* **2021**, *10*, 055008. [CrossRef]
15. Autran, J.L.; Munteanu, D. Atmospheric Neutron Radiation Response of III-V Binary Compound Semiconductors. *IEEE Trans. Nucl. Sci.* **2020**, *67*, 1428–1435. [CrossRef]
16. Jasica, M.J.; Wampler, W.R.; Vizkelethy, G.; Hehr, B.D.; Bielejec, E.S. Photocurrent from Single Collision 14-MeV Neutrons in GaN and GaAs. *IEEE Trans. Nucl. Sci.* **2020**, *67*, 221–227. [CrossRef]
17. Munteanu, D.; Autran, J.L. Terrestrial neutron-induced single events in GaN. *Microelectron. Reliabil.* **2019**, *100–101*, 113357. [CrossRef]
18. Gao, H.; Ahsanullah, D.; Baumann, R.; Gnade, B. A Study of Neutron Induced Single-Event Damage in AlGaN/GaN HEMTs. In Proceedings of the 2022 IEEE Radiation Effects Data Workshop (REDW), Provo, UT, USA, 12–18 July 2022; pp. 1–6.
19. Mirkhosravi, F.; Rashidi, A.; Elshafiey, A.T.; Gallagher, J.; Abedi, Z.; Ahn, K.; Lintereur, A.; Mace, E.K.; Scarpulla, M.A.; Feezell, D. Effects of fast and thermal neutron irradiation on Ga-polar and N-polar GaN diodes. *J. Appl. Phys.* **2023**, *133*, 015704. [CrossRef]
20. Lambert, D.; Parize, J.; Richard, N.; Raine, M.; Duhamel, O.; Marcandella, C.; Losquin, A.; Hemeryck, A.; Inguimbert, C.; Paillet, P. Neutron Displacement Damage cross Section in GaN: Numerical Evaluations and Differences with Si. *IEEE Trans. Nucl. Sci.* **2023**, *70*, 1870–1877. [CrossRef]

21. Yu, C.; Guo, H.; Liu, Y.; Wu, X.; Zhang, L.; Tan, X.; Han, Y.; Ren, L. Simulation study on single-event burnout in field-plated Ga_2O_3 MOSFETs. *Microelectron. Reliabil.* **2023**, *149*, 115227. [CrossRef]
22. Zhang, J.; Dong, P.; Dang, K.; Zhang, Y.; Yan, Q.; Xiang, H.; Su, J.; Liu, Z.; Si, M.; Gao, J.; et al. Ultra-wide bandgap semiconductor Ga_2O_3 power diodes. *Nat. Commun.* **2022**, *13*, 3900. [CrossRef]
23. Berthet, F.; Petitdidier, S.; Guhel, Y.; Trolet, J.L.; Mary, P.; Gaquière, C.; Boudart, B. Influence of neutron irradiation on electron traps existing in GaN-based transistors. *IEEE Trans. Nucl. Sci.* **2016**, *63*, 1918–1926. [CrossRef]
24. Butler, P.A.; Uren, M.J.; Lambert, B.; Kuball, M. Neutron irradiation impact on AlGaN/GaN HEMT switching transients. *IEEE Trans. Nucl. Sci.* **2018**, *65*, 2862–2869. [CrossRef]
25. Gao, H.; Narayan, R.T.; Gnade, B.; Baumann, R. Characterization and simulation of terrestrial neutron induced destructive single-event effects in Gallium Nitride (GaN) power devices. *IEEE Trans. Nucl. Sci.* **2023**, *70*, 2432–2441. [CrossRef]
26. Munteanu, D.; Autran, J.L. Susceptibility of Group-IV and III-V Semiconductor-based Electronics to Atmospheric Neutrons Explored by Geant4 Numerical Simulations. In *Numerical Simulations*; Rao, S., Ed.; IntechOpen: London, UK, 2018; pp. 117–134.
27. Autran, J.L.; Munteanu, D. Radiation Response of Group-IV and III-V Semiconductors Subjected to D–D and D–T Fusion Neutrons. In *New Advances in Semiconductors*; Cavalheiro, A.A., Ed.; IntechOpen: London, UK, 2022; pp. 1–21.
28. Agostinelli, S.; Allison, J.; Amako, K.; Apostolakis, J.; Araujo, H.; Arce, P.; Asai, M.; Axen, D.; Banerjee, S.; Barrand, G.; et al. Geant4—A simulation toolkit. *Nucl. Instrum. Meth. A* **2003**, *506*, 250–303. [CrossRef]
29. Allison, J.; Amako, K.; Apostolakis, J.; Araujo, H.; Arce Dubois, P.; Asai, M.; Barrand, G.; Capra, R.; Chauvie, S.; Chytraceket, R.; et al. Geant4 developments and applications. *IEEE Trans. Nucl. Sci.* **2006**, *53*, 270–278. [CrossRef]
30. Allison, J.; Amako, K.; Apostolakis, J.; Arce, P.; Asai, M.; Aso, T.; Bagli, E.; Bagulya, A.; Banerjee, S.; Barrand, G.; et al. Recent developments in Geant4. *Nucl. Instrum. Meth. A* **2016**, *835*, 186–225. [CrossRef]
31. Coffie, R.L. High Power High Frequency Transistors: A Material's Perspective. In *High-Frequency GaN Electronic Devices*; Fay, P., Jena, D., Maki, P., Eds.; Springer International Publishing: Cham, Switzerland, 2020; pp. 5–41.
32. Yakimov, E.B.; Polyakov, A.Y.; Shchemerov, I.V.; Smirnov, N.B.; Vasilev, A.A.; Vergeles, P.S.; Yakimov, E.E.; Chernykh, A.V.; Ren, F.; Pearton, S.J. Experimental estimation of electron–hole pair creation energy in β-Ga_2O_3. *Appl. Phys. Lett.* **2021**, *118*, 202106. [CrossRef]
33. Gordon, M.S.; Goldhagen, P.; Rodbell, K.P.; Zabel, T.H.; Tang, H.H.K.; Clem, J.M.; Bailey, P. Measurement of the Flux and Energy Spectrum of Cosmic-Ray Induced Neutrons on the Ground. *IEEE Trans. Nucl. Sci.* **2004**, *51*, 3427–3434. [CrossRef]
34. Goldhagen, P. Cosmic-Ray Neutrons on the Ground and in the Atmosphere. *MRS Bull.* **2003**, *28*, 131–135. [CrossRef]
35. Autran, J.L.; Munteanu, D. *Soft Errors: From Particles to Circuits*; Taylor & Francis/CRC Press: Boca Raton, FL, USA, 2015.
36. Brown, D.A.; Chadwick, M.B.; Capote, R.; Kahler, A.C.; Trkov, A.; Herman, M.W.; Sonzogni, A.A.; Danon, Y.; Carlson, A.D.; Dunn, M.; et al. ENDF/B-VIII.0: The 8th Major Release of the Nuclear Reaction Data Library with CIELO-project Cross Sections, New Standards and Thermal Scattering Data. *Nucl. Data Sheets* **2018**, *148*, 1–142. [CrossRef]
37. Chadwick, M.B.; Herman, M.W.; Obložinský, P.; Dunn, M.E.; Danon, Y.; Kahler, A.C.; Smith, D.L.; Pritychenko, B.; Arbanas, G.; Arcilla, R.; et al. ENDF/B-VII.1 Nuclear Data for Science and Technology: Cross Sections, Covariances, Fission Product Yields and Decay Data. *Nucl. Data Sheets* **2011**, *112*, 2887–2996. [CrossRef]
38. Shibata, K.; Iwamoto, O.; Nakagawa, T.; Iwamoto, N.; Ichihara, A.; Kunieda, S.; Chiba, S.; Furutaka, K.; Oyuka, N.; Ohsawa, T.; et al. JENDL-4.0: A New Library for Nuclear Science and Engineering. *J. Nucl. Sci. Technol.* **2011**, *48*, 1–30. [CrossRef]
39. Geant4 General Particle Source (GPS). Available online: https://www.fe.infn.it/u/paterno/Geant4_tutorial/slides_further/GPS/GPS_manual.pdf (accessed on 20 November 2023).
40. Munteanu, D.; Autran, J.L. Modeling and Simulation of Single-Event Effects in Digital Devices and ICs. *IEEE Trans. Nucl. Sci.* **2008**, *55*, 1854–1878. [CrossRef]
41. Coronetti, A.; Alía, R.G.; Lucsanyi, D.; Letiche, M.; Kastriotou, K.; Cazzaniga, C.; Frost, C.D.; Saigné, F. An Analysis of the Significance of the $^{14}N(n,p)^{14}C$ Reaction for Single-Event Upsets Induced by Thermal Neutrons in SRAMs. *IEEE Trans. Nucl. Sci.* **2023**, *70*, 1634–1642. [CrossRef]
42. *JESD89B*; Measurement and Reporting of Alpha Particle and Terrestrial Cosmic Ray-Induced Soft Errors in Semiconductor Devices. JEDEC: Arlington, VA, USA, 2021.

Disclaimer/Publisher's Note: The statements, opinions and data contained in all publications are solely those of the individual author(s) and contributor(s) and not of MDPI and/or the editor(s). MDPI and/or the editor(s) disclaim responsibility for any injury to people or property resulting from any ideas, methods, instructions or products referred to in the content.